COSHER joint industry project: Large scale pipeline rupture tests to study CO2 release and dispersion

10 authors, including:

Mohammad Ahmad
DNV GL
7 PUBLICATIONS **200** CITATIONS

Gelein M de Koeijer
Equinor ASA
36 PUBLICATIONS **1,568** CITATIONS

Sandra Hennie Nilsen
Equinor ASA
14 PUBLICATIONS **192** CITATIONS

Carlo Maria Spinelli
Eni SpA
18 PUBLICATIONS **122** CITATIONS
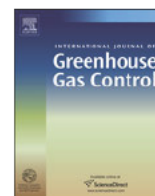
COSHER joint industry project: Large scale pipeline rupture tests to study CO$_2$ release and dispersion

Mohammad Ahmad [a,*], Barbara Lowesmith [a], Gelein De Koeijer [b], Sandra Nilsen [b], Henri Tonda [c], Carlo Spinelli [d], Russell Cooper [e], Sigmund Clausen [f], Renato Mendes [g], Onno Florisson [a]

[a] DNV GL, The Netherlands
[b] STATOIL, Norway
[c] TOTAL, France
[d] ENI, Italy
[e] National Grid, UK
[f] GASSCO, Norway
[g] PETROBRAS, Brazil

ARTICLE INFO

ABSTRACT

The COSHER joint industry project involved the conduct of large scale experiments to provide release and dispersion data under well-defined conditions, studying the full bore rupture of a CO$_2$ dense phase high pressure underground pipeline at large scale. The data generated are useful for model development and validation as well as for better understanding of the risks due to large scale underground CO$_2$ pipeline ruptures. In order to simulate the depressurization of a pipeline, a 219.1 mm diameter pipeline loop was fed from both ends by a 148 m^3 reservoir of CO$_2$. The rig was designed to promote outflow in the liquid phase for as long as possible. About 136 ton of CO$_2$ were released in 204 s. During the experiments, measurements of the fluid pressure, fluid temperature and wall temperature of the test facility were made together with measurements of the CO$_2$ concentration contours and temperature within the dispersing gas cloud.

© 2015 Published by Elsevier Ltd.

1. Introduction

The capture of carbon dioxide (CO$_2$) from power plants and other large CO$_2$ point sources has become relevant within the concept to mitigate CO$_2$ emissions via carbon capture and storage (CCS) (Metz et al., 2005). A big part of this captured CO$_2$ stream will be transported at high pressure liquid phase conditions and stored in aquifers or in offshore underground depleted oil and gas fields, or used for enhanced oil or gas recovery.

The use of high pressure CO$_2$ transmission pipelines is classified as having a major hazard potential according to an EC study (Pipeline Safety Instrument for Involving Pipelines, 1999). CO$_2$ is asphyxiating and is a heavy gas. The maximum CO$_2$ concentration an adult can be exposed to for 8 h is 5000 ppm (ACGIH, 1991), while the exposure to a CO$_2$ concentration of 10% will lead to

unconsciousness in just 1 min (Pohanish and Greene, 1996). The present experience in operating CO$_2$ pipelines is limited one off-shore pipeline in Northern Norway (Hansen et al., 2013) and to those used for enhanced oil recovery (CRS, 2007). The UK Health and Safety Executive (HSE) has simulated the releases of CO$_2$ from vapor pipelines due to a puncture or a rupture, and concluded that distances to specified risk contours around vapor CO$_2$ pipelines are roughly comparable to natural gas pipelines (McGillivray and Wilday, 2009). Pipeline operators need to demonstrate to regulatory authorities that the risks are well understood and that such CO$_2$ pipelines can be operated safely. However, the processes that determine the hazards posed by intentional or accidental releases of CO$_2$ from pipelines are complex due to the thermodynamics of the CO$_2$ outflow, with changes of phase, followed by the dispersion of the cold heavy gas.

The release and dispersion of CO$_2$ from high-pressure pipelines have been examined in a big number of recent publications. DNV Software has investigated CO$_2$ release and dispersion modeling. Witlox et al. (2009) have upgraded the existing discharge model in PHAST version 6.53.1 to account for the effects of solid CO$_2$,

* Corresponding author at: 17 Energieweg 9743AN, Groningen, The Netherlands.
Tel.: ██████████.
E-mail address: ████████████@dnvgl.com (M. Ahmad).

Fig. 1. The pipeline loop (plan view).

Fig. 2. The pipeline loop (viewed from the east).

ensuring that during CO_2 expansion into atmospheric conditions, the equilibrium followed the sublimation curve rather than extrapolating the evaporation curve. The model was validated against experimental data; however, measurements were not shown due to confidentiality. In another paper, Witlox et al. (2011) have released the results of sensitivity tests for both liquid and supercritical CO_2 releases from vessels and pipes with the revised PHAST version 6.6 model. E.ON in UK has also released several studies in the framework of their CCS research program. Mazzoldi et al. (2008a,b, 2011) have studied atmospheric dispersion from pipeline and vessel releases, modeling only gaseous discharge and comparing simulation from the heavy gas model ALOHA to the CFD model Fluidyn–Panache. Hill et al. (2011) have carried out CFD and PHAST simulations of dense phase CO_2 from 0.5 m diameter hole in a pipeline located above ground level. No comparison with experimental data was performed.

There is however, a considerable modeling work on CO_2 free jets and dispersion that was validated. Dixon et al. (2012) have studied

free releases of dense phase CO_2 simulating leaks from aboveground CO_2 pipes using three different models, FRED, OpenFOAM and CFX. The Bernoulli equation used in the three models provided reasonable predictions of the mass release rates. The plume widths were slightly better predicted by FRED that did not simulate solid particles; however, the CFD models were noted to be in general better after comparison against experimental data. The University of Leeds has developed a mathematical model with a composite equation of state for modeling CO_2 near field sonic dispersion (Wareing et al., 2012, 2013) predicting the thermo-physical properties of the three phases. They have later validated the model against an experimental data set simulating free releases into air (Woolley et al., 2013; Wareing et al., 2014a) as well as releases from punctures in buried pipelines (Wareing et al., 2014b). Woolley et al. (2014) have used an integrated multi-scale approach to model CO_2 discharge and dispersion in realistic terrain. Validated against controlled releases from a lab-scale experimental rig, the approach appeared to have certain limitation as the models are integrated

Fig. 3. Arrangement of oxygen cells at 1 m above local ground level.

in a linear fashion with no feedback between them. Brown et al. (2014) have developed a homogeneous relaxation model to simulate outflow following the full bore rupture of dense phase CO_2 pipelines. The phase behavior data was obtained using a cubic equation of state and the delayed liquid–vapor transition was accounted for using an empirically derived equation for the relaxation time to thermodynamic equilibrium. The comparison of the predictions with experimental CO_2 pipeline rupture data produced reasonable agreement.

Several experimental research programs have been launched to provide experimental data to support the development of models for the determination of safety zones of CO_2 transmission pipelines and to improve the understanding of the release and leakage hazards. One of these programs is the COOLTRANS research program set by National Grid (Coooper, 2012) with the objective to address knowledge gaps related to the safe design, construction and operation of dense phase CO_2 pipelines. The program includes theoretical studies as well as experimental investigation (shock tube tests, vent and puncture tests, crack propagation tests). The program of shock tube tests on CO_2 mixtures was launched in order to understand the decompression behavior of CO_2 following a pipeline failure (Cosham et al., 2012). COOLTRANS has provided experimental data for many of the previously mentioned modeling works. Another program is the CO_2PipeHaz project[1], a consortium to develop and test mathematical models for safety assessment of CO_2 pipelines with some lab-scale release experiments conducted. A recent experimental investigation was carried out by Ahmad et al. (2013) within the framework of the Dutch national CCS research program (CATO2) to study CO_2 outflow at small scale from small orifices (simulating punctures) in a high pressure vessel. In this study, the impact of varying the release orifice diameter and the initial vessel pressure on the CO_2 discharge were examined, and the different thermodynamic regimes inside the high pressure vessel and in the outflow zone were described. CO_2 PIPETRANS is a joint industry project (JIP) led by DNV GL with a main work package dedicated to generating experimental data to

assist the development and validation of dense phase CO_2 depressurization, release, and dispersion models. The data generated in this JIP[2] were made public. A set of a large scale experiments was conducted where mainly the dispersion characteristics of CO_2 were measured under different conditions (different initial temperature and pressure conditions, different orifice size, release orientation and impact on target). A coriolis flow meter was later added in a second set of experiments for more accurate flow rate measurements with a bigger set of temperature and concentration sensors installed down to 80 m from the release point.

Despite the large amount of studies and published literature investigating CO_2 release and dispersion, the availability of additional reliable data based on realistic scale pipeline rupture tests to allow model validation is useful. This paper presents some data from the COSHER JIP. COSHER stands for CO_2 safety, health, environment and risk. In this project, large scale pipeline rupture tests were performed simulating loss of containment and subsequent dispersion of CO_2 as a result of a rupture arising from third party interference. The project involved the conduct of two large scale experiments to provide data under well-defined conditions studying the full bore rupture of a CO_2 dense phase high pressure underground pipeline. In order to simulate a very long pipeline, a 219.1 mm diameter pipeline loop 230 m long was fabricated with both ends of the loop connected to the underside of the lower end of a 1320.8 mm diameter reservoir, 117 m long and inclined at 0.5°. This is the largest experimental program on CO_2 as far as the authors know of. The rupture release experiments were conducted in different wind speed conditions. During the experiments, a ground crater was formed and the CO_2 was allowed to flow freely from both ends of the ruptured section of the pipeline. Measurements of the fluid pressure, fluid temperature and wall temperature of the test facility were made together with measurements of the dispersing gas cloud.

---

[1] http://www.co2pipehaz.eu/.

2. Experimental arrangement

The tests were conducted on the DNV-GL Test Site at Spadeadam in Cumbria, UK. The experimental test facility comprised a large reservoir formed from a 117.1 m long, 1320.8 mm diameter steel pipeline connected to a 226.6 m long pipeline loop formed from 219.1 mm diameter steel pipe. A schematic of the arrangement is shown in Fig. 1. The test facility was below ground level. The section to be ruptured was located in the center of a 94 m straight section of pipe as shown in Fig. 1. The arms of the pipeline loop came up from under the reservoir to about 0.5 m below ground level (Fig. 2). The reservoir had a total volume of 148.75 m³ and the loop had a volume of 6.68 m³ giving a total rig volume of 155.43 m³.

The gas reservoir and pipeline loop were pressurised with pure CO_2 (99.99%) to nominally 15 MPa. When full, the test rig contained about 150 ton. A shaped explosive charge was laid on the top dead center of the spool in the center of the pipeline loop for a length of about 3.3 m. At each end of this length, the shaped charge was installed around the pipe circumference for about ¾ of its length. The objective was to achieve a clean cut and produce a release from each side of the rupture from the full bore of the pipe.

When suitable weather conditions were prevailing (a nominally westerly wind), activation of the explosive charge initiated the release of CO_2 which flowed freely from the test rig. In order to protect the reservoir from excessively low temperatures, and to provide the option to terminate in an emergency, the ball valves on either side of the rupture were to be closed when the wall temperatures measured near the reservoir outlet reached −25 °C, indicating that the reservoir was nearly empty of liquid CO_2. The activation time of the ball valves is 5 s and so is its closure rate. Table 1 summarizes some dimensional and constructional information concerning the test rig.

3. Scientific measurements

During the tests, a large number of measurements were made. On the test facility, the pressure, fluid temperature and wall temperatures were recorded. These measurements were located on the reservoir (east and west end) and at several locations either side of the rupture, on the straight section of the pipeline loop. In addition, a measurement of differential pressure across the reservoir was attempted, aimed at determining the liquid level in the reservoir (and hence mass outflow). In the reservoir, pressure was measured at two locations, one at the west end on a blanked 12" NB outlet and the other at the east end at a 1¼" tapping, using Druck UNIK 5000 series transducers with a range of 0–16 MPa and a stated accuracy of ±0.08% of full scale. The pressure in the pipeline loop was measured at a total of 12 locations, 6 either side of the rup-

Table 1
Summary of dimensional and constructional information of the rig.

	Reservoir	Loop
Steel	API-5LX80	A333 grade 6
Outside diameter	1320.8	219.1
Wall thickness	25.8	12.7
Internal diameter	1269.2	193.7
Surface roughness	–	Range: 7.8–3.7 μm Ra. Average: 5.5 μm Ra
Length	117.1 m (between dome ends)	226.6
Dome end volume (each)	0.3 m³	–
Reservoir slope	0.494°	0
Volume	148.752 m³	6.677 m³
Total volume	155.429 m³	

Table 2
Summary of the test conditions prior to rupture.

Rig conditions	Test
Overall average gage pressure (MPa)	15.08
Average fluid temperature in reservoir (°C)	13.1
Average wall temperature of reservoir (°C)	14.2
Estimated inventory (tons)	146.8
Atmospheric conditions	
Wind direction (degrees relative to grid N)	261
Wind speed (m s⁻¹)	1.9
Ambient temperature (°C)	17.4
Atmospheric pressure (Pa)	99700
Relative humidity (%)	71.5

Fig. 4. The visible cloud at 10 s (top), 30 s and 120 s (bottom) after the rupture.

ture. At two positions, high frequency pressure transducers with a range of 0–20 MPa were used. These were manufactured by Kulite (Type CTL-3-375M-200BARSG), with a natural frequency of at least 1.4 MHz and an accuracy of ±0.5% of full scale. At the other locations in the pipeline loop, Druck UNIK 5000 series transducers with a range of 0–16 MPa and a stated accuracy of ±0.08% of full scale were used. The instruments were calibrated on site using a Druck pressure calibrator before the test and again after the test. The pressure

Reservoir Pressure
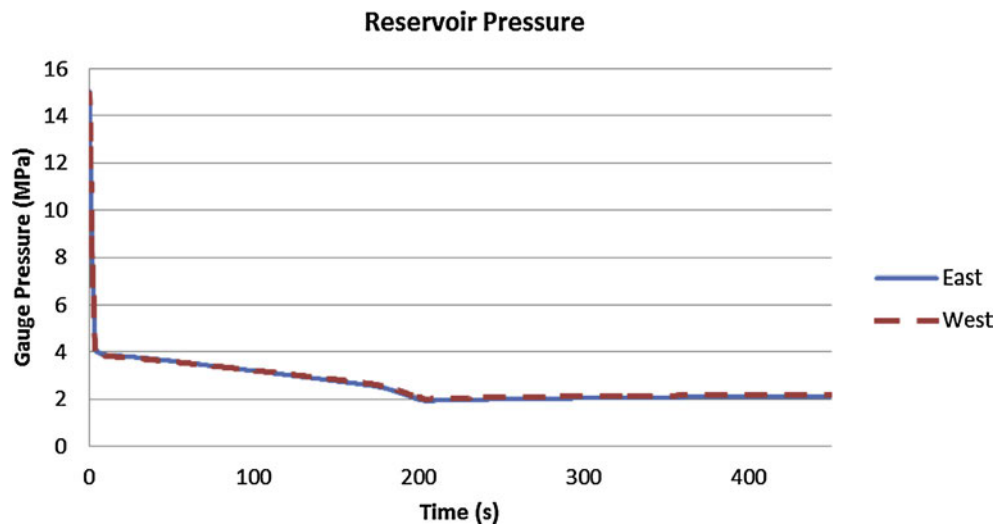
Fig. 5. Pressure in the reservoir.

Reservoir Fluid Temperature
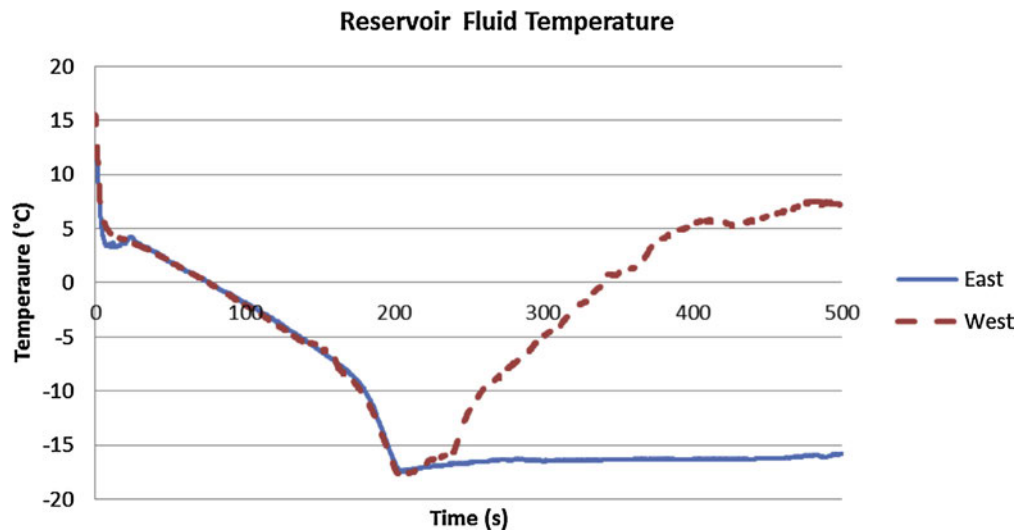
Fig. 6. Temperature inside the reservoir.

measurements were logged at 10 Hz on a SPARTAN data acquisition system and the results provided in engineering units of gage pressure in MPa. The signals were also recorded on a high speed data acquisition system at 100 kHz (Hi-Techniques SYNERGY system).

The fluid temperature was measured at two locations in the reservoir, one close to the west end of the reservoir, inserted about 100 mm from the top of the pipe and other at the east end, inserted about 100 mm from the bottom of the pipe. The instruments were 1.5 mm diameter mineral insulated stainless steel sheathed Type T thermocouples. The wall temperature of the reservoir was measured using welded tip, PTFE insulate, Type T thermocouples, spot welded to the outer pipe wall. The fluid temperature was also measured in the pipeline loop at 12 locations, 6 either side of the rupture. Two of these instruments were positioned on the sweepolet connections, inserted about 3 mm through the side wall of the pipe. The other 10 were located either side of the rupture. The instruments were inserted about 3 mm through the bottom of the pipe. In all cases, 1.5 mm diameter mineral insulated stainless steel sheathed, Type T thermocouples were used, supplied with a certificate of conformity. The temperatures were logged on a SPARTAN data acquisition system at 10 Hz. The results were provided in engineering units of degrees Celsius.

In the field, measurements of concentration at more than 70 locations (Fig. 3) up to 700 m from the rupture location were made using 73Citicell AO$_2$ oxygen cells were used to determine oxygen depletion, and hence CO$_2$ concentration. Fifty-nine were located 1 m above local ground level and fourteen at 1.8 m above local ground level.

The oxygen cells output a nominal voltage of 10 mV when in air, which reduces linearly with oxygen depletion, which can then be translated into CO$_2$ concentration. The data was post-processed such that the average of each oxygen cell output during the 30 s prior to rupture was taken to correspond to 0% CO$_2$ for that oxygen cell. The oxygen cells are temperature compensated, but their output varies slightly with temperature. The manufacturer states that the variation is less than 2% over range 0–40 °C. Taking this variation to be ±1% of the reading in air (nominally 10 mV), corresponds to ±0.1 mV. This corresponds to ±1CO$_2$. So the accuracy of the dispersion measurements can be considered to be accurate to an absolute value of ±1%.

The temperature in the dispersing gas cloud was determined using an array of 52 thermocouples formed from PTFE insulated Type T thermocouple wire, twisted at the ends to make a joint. These thermocouples were deployed close to the majority of the
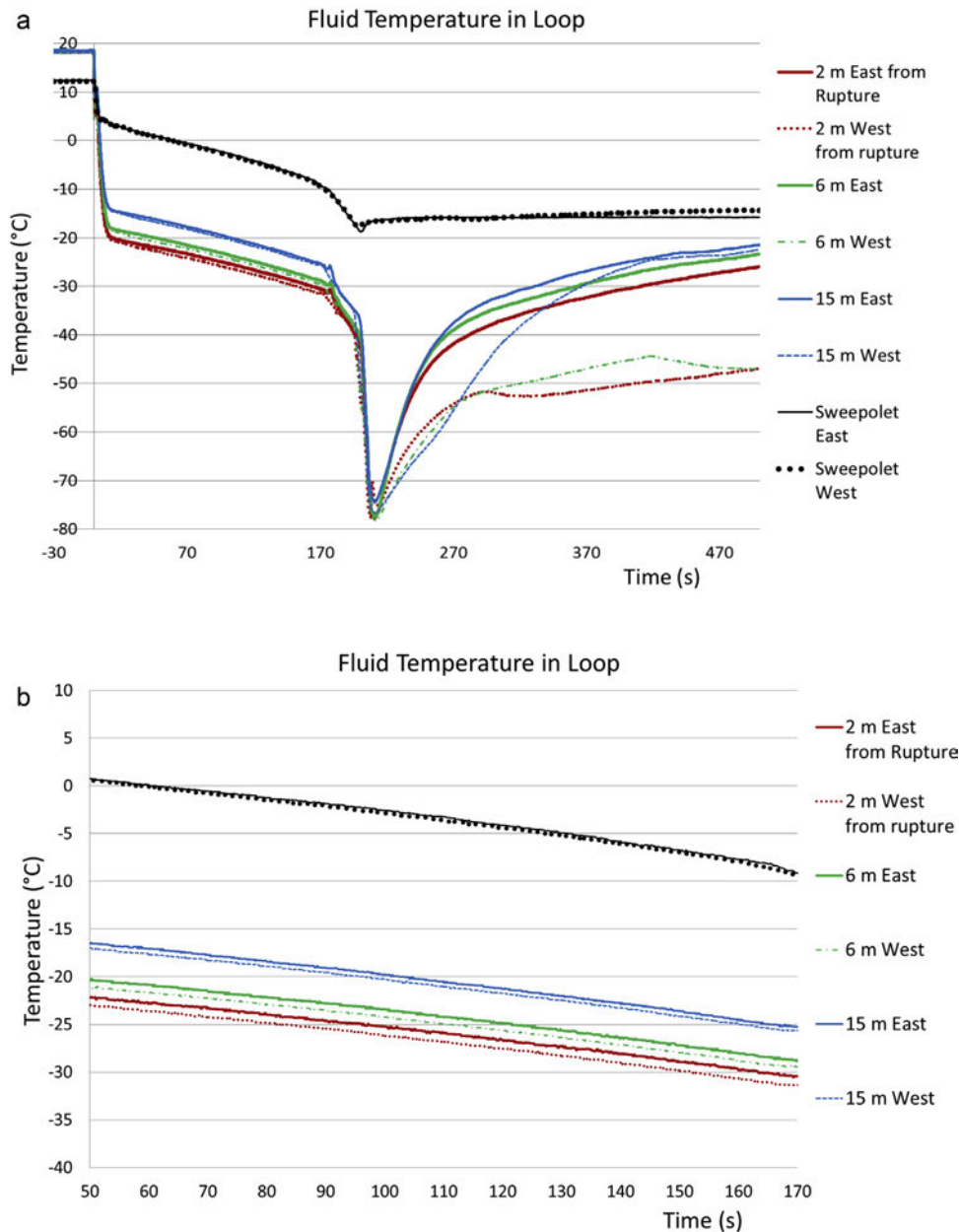
Fig. 7. (a) Temperature in the 219.1 mm pipeline loop (the sweepolets are 113.3 m from the rupture location). (b) Temperature in the 219.1 mm pipeline loop between 50 and 170 s.

oxygen cells at 1 m and 1.8 m above ground level within 200 m of the rupture location. These instruments were logged at 10 Hz on one of several SPARTAN data acquisition systems and the results provided in engineering units of degrees Celsius.

The atmospheric pressure, temperature and relative humidity and solar radiation were measured prior to and throughout the test. A UNIK 5000 series 0–0.16 MPa (abs) transmitter was used for the atmospheric pressure, a Type T thermocouple for the temperature and a Hygroclip2 proprietary pre-calibrated instrument manufactured by Omni Instruments was used for the humidity. A Kipp & Zonen CMP3 pyranometer was used to measure the background solar radiation. The wind speed and direction was measured at many locations using a Gill Windsonic, 2-direction sonic anemometer. All these instruments were recorded at 10 Hz on a SPARTAN data acquisition system and results provided in appropriate engineering units.

Extensive video footage included close up views of the rupture location with high speed video and a thermal imaging (IR) camera. Aerial footage was taken from cameras attached to a helium balloon.

4. Test conditions

The rupture test presented here was carried out in relatively low wind conditions (the prevailing wind speed was about 2 m s^{-1}) with an atmospheric temperature of 17.4 °C and a fluid temperature inside the rig of 13 °C. The test conditions are summarised in Table 2.

For all tests, the explosive charge produced a clean cut and allowed unobstructed outflow from each end. Upon rupture, CO_2 and soil were ejected into the air, significant debris throw was observed for about 25–30 s and then small amounts of soil con-
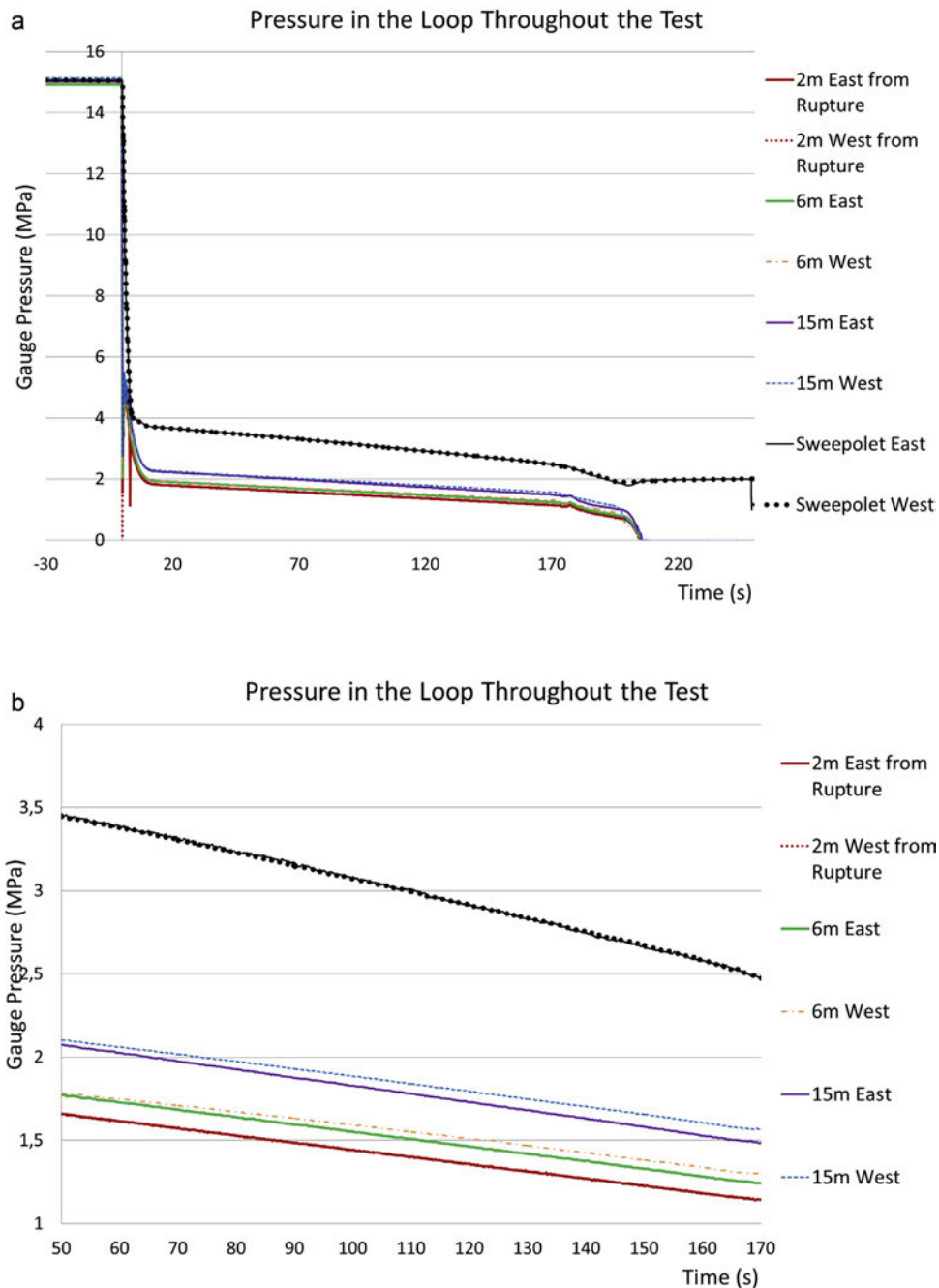
Fig. 8. (a) Pressure in the 219.1 mm pipeline loop. (b) Pressure in the 219.1 mm pipeline loop between 50 and 170 s.

tinued to be ejected until about 60 s after the rupture. After that no further ejection of soil was apparent.

5. Test description

During the presented test, the initial rupture produced a visible plume projecting vertically into the air. Initially this was predominantly vertically but the plume also soon spread width-wise. At 10 s after the rupture, the plume was about 50 m high and 125 m wide. The plume reached a maximum visible height after 20 s of about 60 m. At this time, the plume ejected to the north and south fell to the ground and started to form a low level blanket which spread north, south and east. After about 1 min, there was also significant spread of the cloud blanket in the upwind direction (west). The release became more noisy at around 175 s, coinciding with the

time at which the pressure began to drop more quickly, probably indicative of gas phase outflow at the exit.

The wall temperatures on the reservoir outlets (sweepolets) was about −27 °C by 170 s, so the test had to be terminated by closing the valves on either side of the rupture. The valves had closed by 204 s although a small leak persisted through the valve on the east side of the rupture. After termination of the test, the central region of the visible cloud around the rupture location began to disappear but the remainder of the cloud took a considerable time (6–8 min) to disperse, particularly in the regions of the cloud to the north and south which occupied the low level areas around the streams which run parallel to the site boundary. It took about 12 min before all the visible cloud had disappeared. The ground crater formed at the rupture was about 5 m across in both directions and was up to 1.25 m deep. Fig. 4 shows the visible cloud as viewed by an
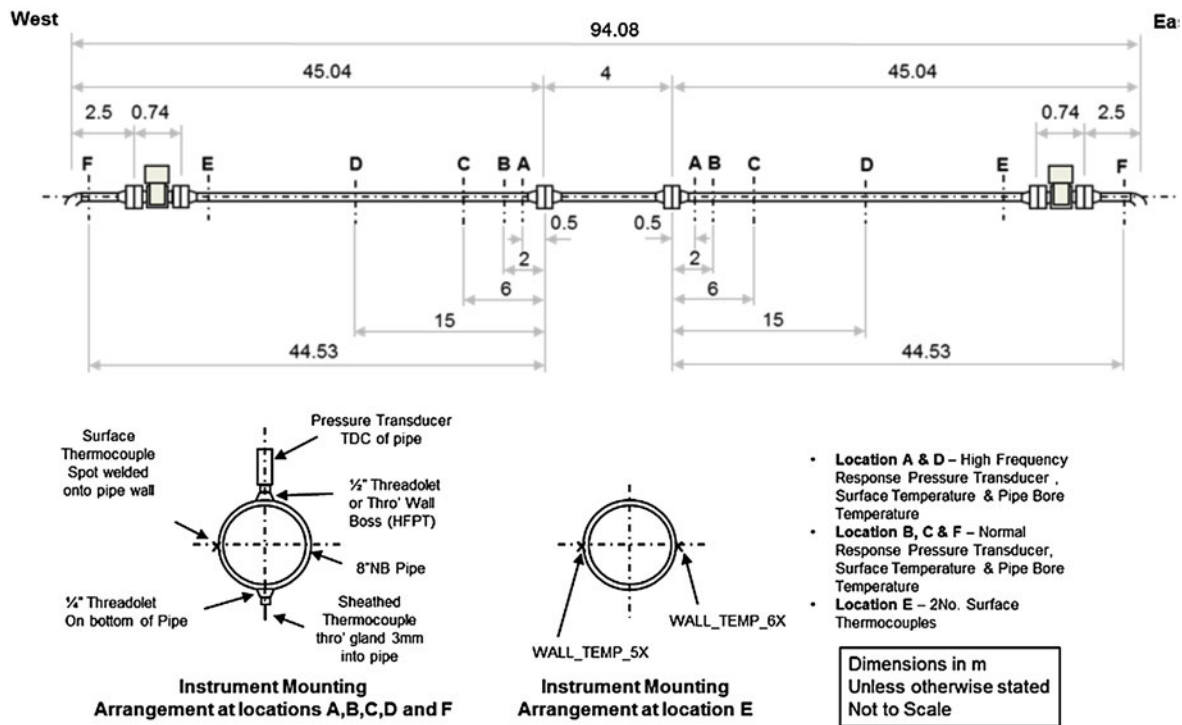
Fig. 9. Instrument locations either side of the rupture.

6. Pressure and temperature in the test rig

Fig. 5 presents the reservoir pressure during the test. Starting from initially liquid conditions in the reservoir, the pressure inside the vessel drops very fast after the release onset to reach saturation conditions within 4.2 s. It is assumed that the saturation phase starts when the pressure drop rate inside the vessel slows as the effect of mass released is then partially compensated for by the boiling liquid inside the vessel. The saturation phase starts at 4.07 MPa and at about 4.5 s from the release onset.

The temperature was measured at east and west end inside the reservoir. The fluid temperature throughout the test is shown in Fig. 6. The temperature sensor in the reservoir at the east end was near the bottom of the reservoir, whereas at the west end was near the top of the reservoir. The minimum fluid temperature recorded was −17.8 °C.

After filling the rig and before the start of the test, a slight difference in temperature was observed between the upper-western side of the reservoir and the lower-eastern side. A similar temperature drop profile was recorded at both sides of the reservoir during the steady state period. A divergence in temperature at the west and east ends of the reservoir starts to occur around 215 s after the termination of the test. Heat coming from the surrounding caused the increase in temperature at the west end while a continued slight leakage of gas through the valve on the east side of the loop, (gas continues to leave the reservoir via the sweepolet) had maintained low temperature at that end of the reservoir.

The fluid temperature was measured at 12 locations on the pipeline loop, 6 either side of the rupture (Fig. 9). Fig. 7a and b shows the fluid temperature measured at 3 locations either sides of the rupture and at the sweepolets. The fluid temperature drop

had same profile on both sides of the rupture during the release with a minimum fluid temperature of about −78 °C measured at 2 m from the release location. The good agreement between the west and east sides was apparent until valve closure occurs. The continued slight leakage of gas through the valve on the east side of the loop resulted in higher fluid temperature than those recorded at the West side. The presence of a certain vapor speed due to the leakage on the East side resulted in higher overall heat transfer coefficient with the surrounding.

Fig. 8a and b shows the pressures during the pseudo-steady period and the final period, respectively, using the 10 Hz data. At about 204 s, the valves had closed and hence the short length of pipe between the valves and the rupture quickly depressurized, but increased at the sweepolets (behind the valve).
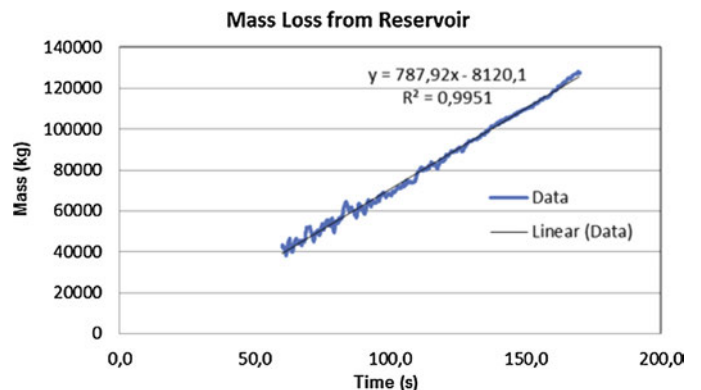
Fig. 10. Mass loss from the reservoir determined from differential pressure measurements.
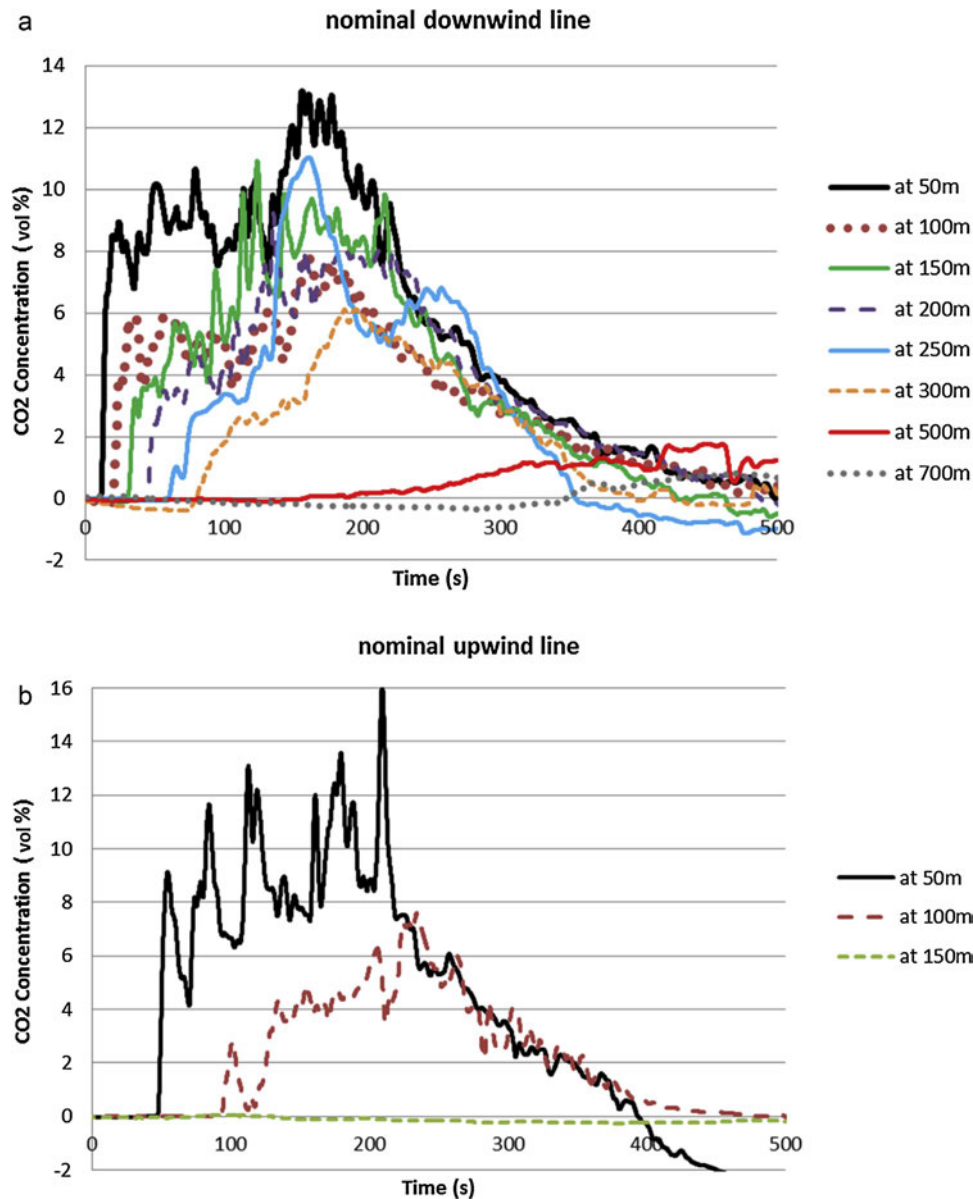
Fig. 11. Concentrations at 1m above ground on a nominal downwind line 90° relative to grid N (top) and on nominal upwind line 270° relative to grid N (bottom).

7. Mass outflow during the pseudo-steady period

A differential pressure measurement from the top of the west end of the reservoir to the bottom of the east end of the reservoir was attempted. This pressure would provide a measure of the height of the liquid level in the reservoir, from which the rate of mass outflow during the pseudo-steady period could be determined. During the test, the mass release rate was estimated by taking the initial rig inventory (146.8 ton). The liquid ran out at about 180 s, leaving about 10.2 ton in the reservoir. Hence the estimated pseudo-steady mass release rate was (146,800 – 10,200)/180 = 758 kg s^{-1}. However, measurements of differential pressure were achieved for the period between 60 and 170 s after the rupture. Using these data, the height of liquid in the reservoir with time was calculated and from that the mass loss from the reservoir with time.

Fig. 10 shows that the gradient (and hence release rate) is approximately constant between 60 and 170 s. A straight line fit to this section of data (with a correlation coefficient of better than 0.99) gives a release rate of 788 kg s^{-1}. This suggests that the outflow during the saturation phase is steady.

8. Gas concentrations

Figs. 11 and 12 show the CO$_2$ concentrations with time measured at 1 m above local ground level on different radial lines downwind and upwind from the rupture locations. The gas concentration data from the oxygen cells was post-processed by applying a 3 s rolling average to eliminate short duration fluctuations.

Gas was detected downwind, upwind and crosswind from the rupture location. For the first 250 m, the time of gas arrival downwind correlated linearly to distance = 4.05 × time, with a correlation coefficient of 96%, suggesting the speed of the gas cloud was about 4 m s^{-1}, despite the wind speed being about 2 m s^{-1}. This difference is due to the gravitational slumping of the cold CO$_2$ after ejection from the crater. At greater distances, the speed of

30° north of the nominal downwind line

45° north of the nominal downwind line
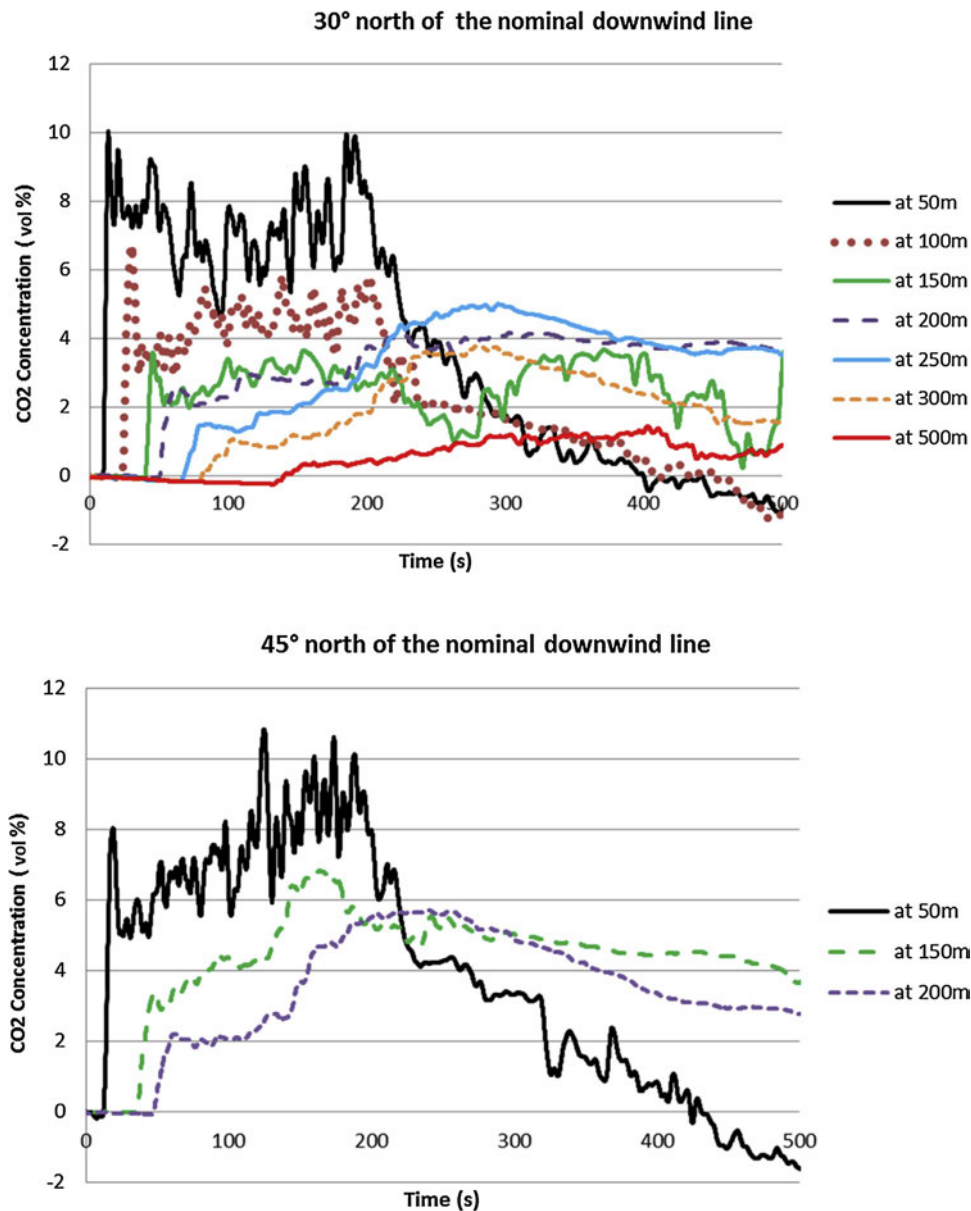
Fig. 12. Concentrations at 1 m above ground on a downwind line 60° relative to grid N (top) and on downwind line 120° relative to grid N (bottom).

spread slows down. As can be seen in the figures below, the time of arrival of the gas, increases with increasing distance.

Within 100 m of the release location (Fig. 11), the range of pseudo-steady concentrations was similar for the upwind and downwind directions and that is mainly because of the low wind speed and because of the high influence of the jet momentum and behavior at the rupture location on the dispersion and the CO_2 concentration contours in the close field. However, as can be also shown in Figs. 11 and 12, for many radial lines in the far field (over 200 m) and at larger distances, the pseudo-steady concentrations were not reached. This is due to the low wind speed and the relatively short duration of the presented test. In the far field (as shown Figs. 11 and 12), the highest concentrations were seen after termination of the release as the pseudo-steady gas cloud had not reached this distance prior to termination of the test. During the first test at a higher wind speed, pseudo-steady CO_2 concentrations were observed at all field locations. After the closure of the ball valve

at around 200 s, the CO_2 concentration in the near field drops more quickly than in the far field because of the relatively high wind speed.

9. Temperature in the gas cloud

The temperature in the dispersing gas cloud was determined using an array of 52 thermocouples (numbered FT01 to FT52) formed from PTFE insulated Type T thermocouple wire, twisted at the ends to make a joint. These thermocouples were deployed close to the majority of the oxygen cells at 1 m and 1.8 m above ground level within 200 m of the rupture location. These instruments were logged at 10 Hz on one of several SPARTAN data acquisition systems and the results provided in engineering units of degrees Celsius. Figs. 13 and 14 show the temperature measurements 1 m above ground on arcs 50 and 100 m from the release point. Fig. 15 shows the arrangement of thermocouples 1 m above the local ground level.

Temperature 1m above ground 50m crosswind and upwind

Temperature 1m above ground on arc 50m downwind
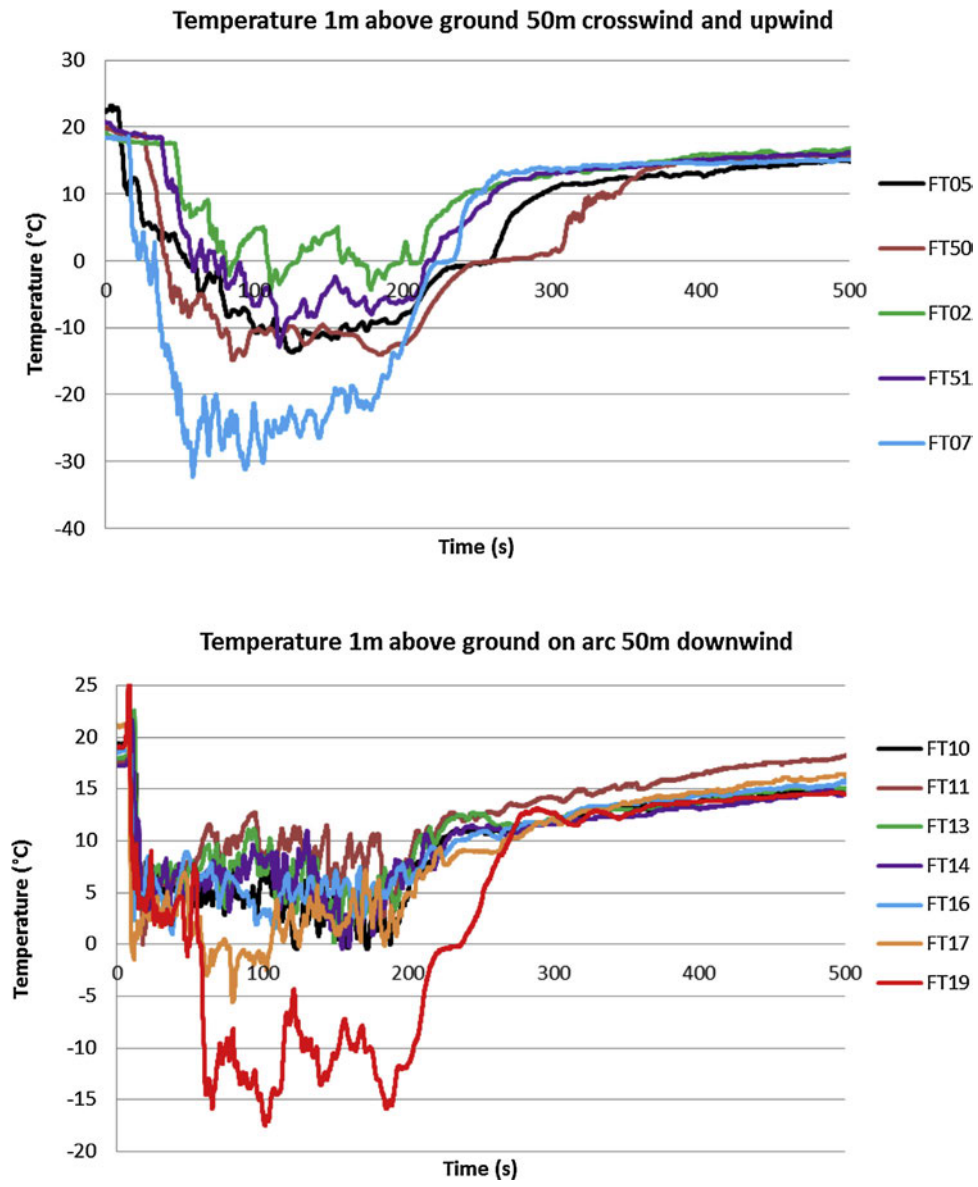
Fig. 13. Temperature inside the gas cloud 1 m above ground on an arc 50 from the release point.

Temperature 1m above ground on arc 100m downwind
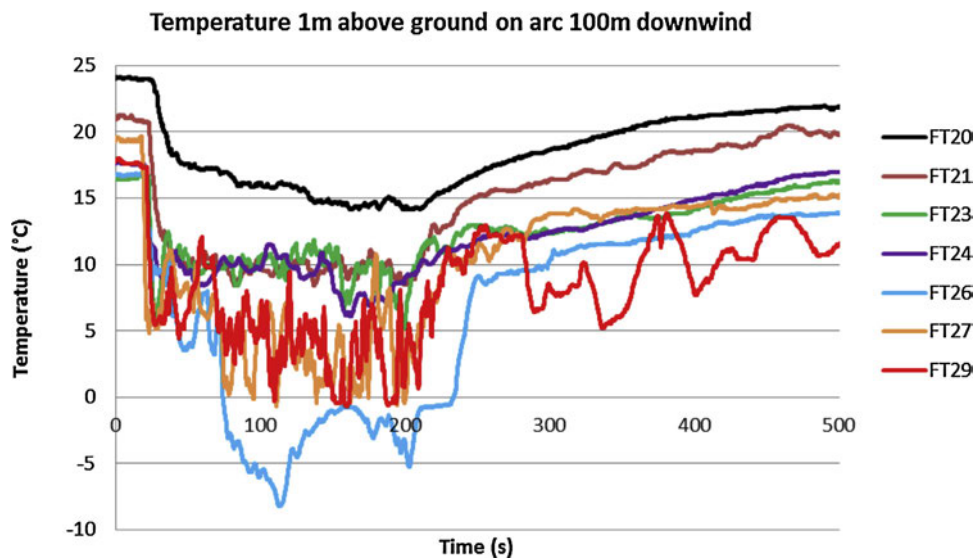
Fig. 14. Temperature inside the gas cloud 1 m above ground on an arc 100 downwind.
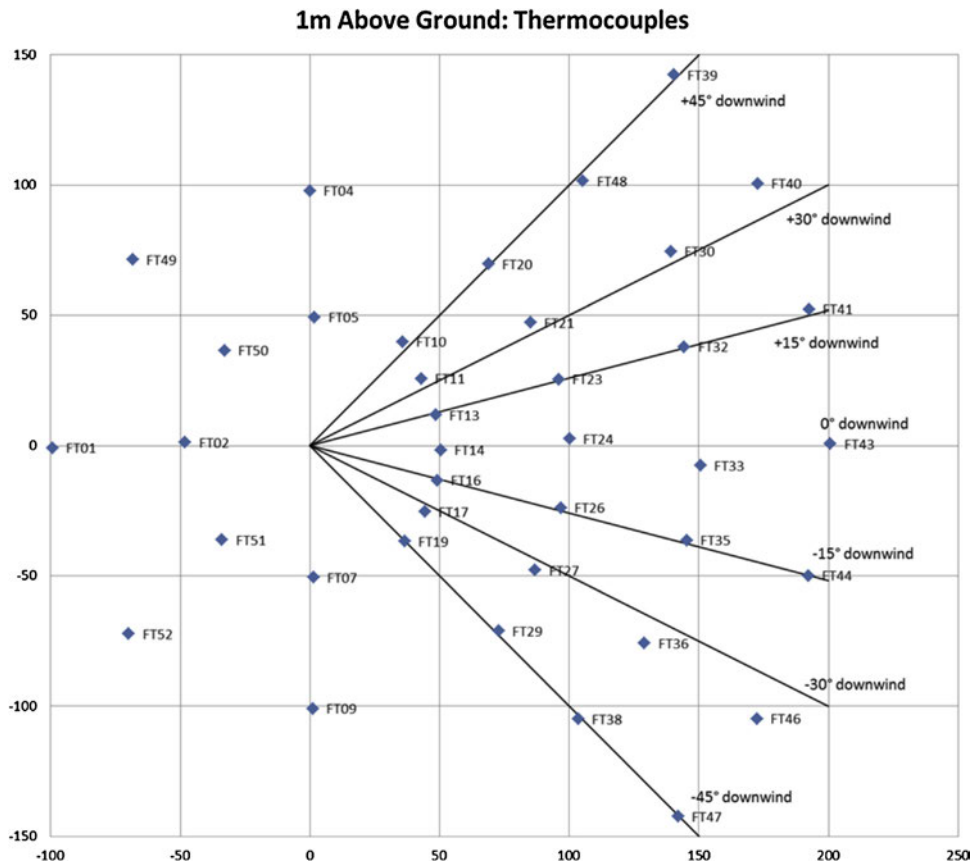
Fig. 15. Arrangement of thermocouples 1 m above local ground level.

Fig. 16. Photograph of the crater and ruptured pipe.
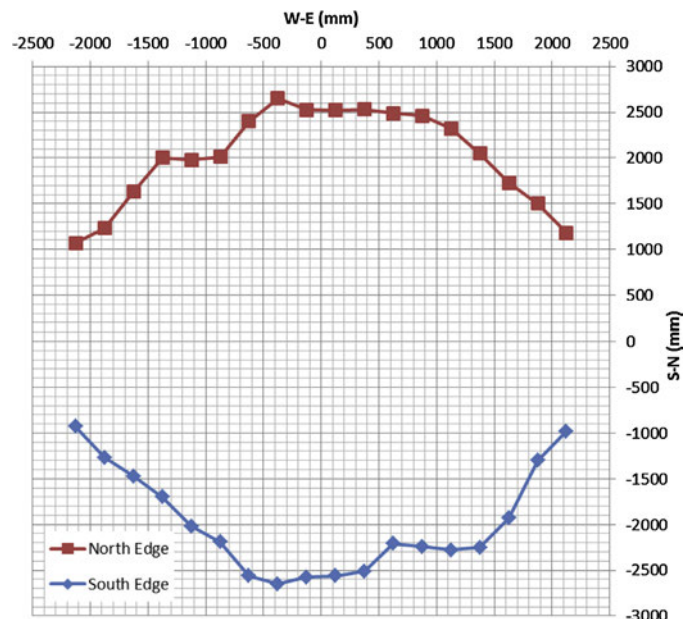
Fig. 17. Shape of the ground crater in plan view.

10. Crater formation

A ground crater was formed by the release. Most soil was ejected within the first 30 s and no soil ejection was identifiable after 60 s. A photograph of the crater is shown in Fig. 16. The ground crater was surveyed to provide a profile of the crater edge (Fig. 17). The depth of the crater was surveyed on several sections from west to east, as shown in Fig. 18.

A region around the crater was covered with a thin white coating. This extended about 2 m west and east of the center of the crater. To the south, the white area extended about 14 m from the center of the crater and to the north about 5 m. The stones were very cold, but the thin coating was predominantly haw-frost which

North-South Profiles of the Crater Depth at Several Locations in the X Direction

North-South Profiles of the Crater Depth at Several Locations in the X 79 Direction
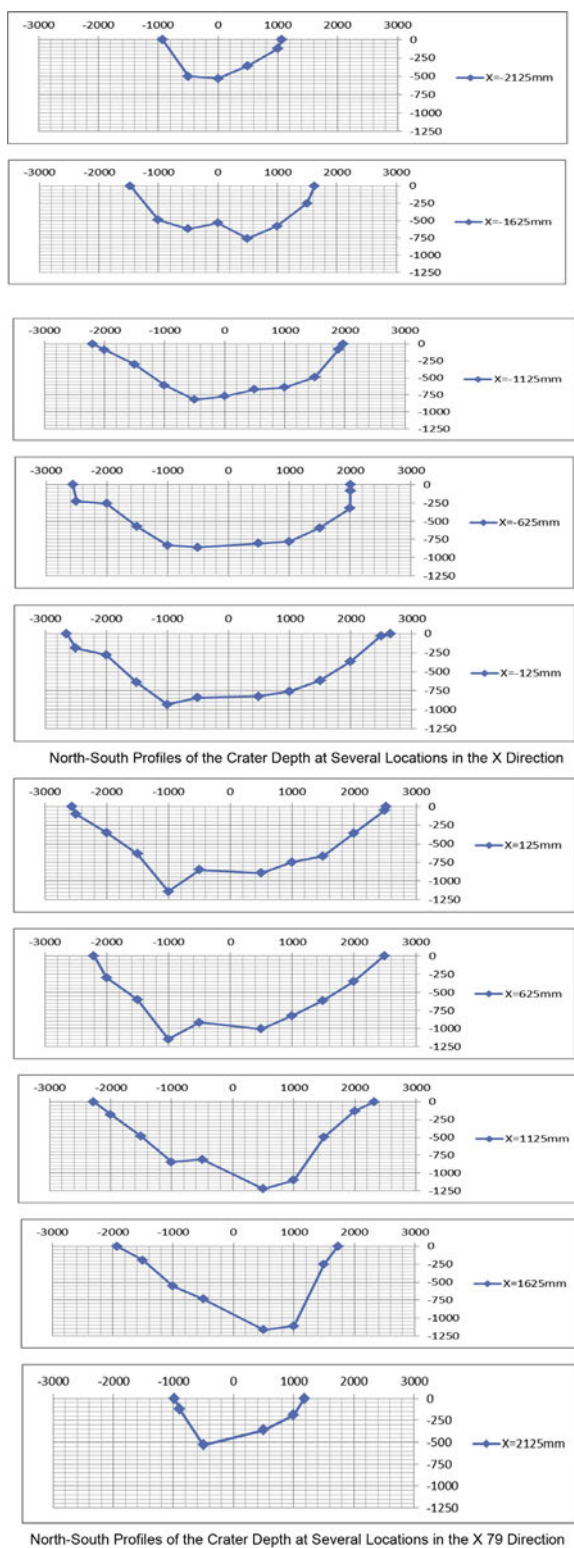
Fig. 18. North–South profiles of the crater depth at several locations in the X direction.

melted to water. No accumulation of CO_2 was found within the crater, although the pipework was encrusted with haw-frost.

11. Conclusions

The paper presents some data from one large scale pipeline rupture test carried out in the COSHER JIP in relatively low wind conditions (about 1.9 m/s). It is most likely the largest one documented. From the data presented in this paper, the following main conclusions can be made:

1. The rupture produced a visible plume that reaching a maximum height of about 60 m and then forming a low level blanket reaching areas 400 m far from the rupture location.
2. A fast drop in pressure is observed in the rig after the release onset from the initial high pressure sub-cooled liquid conditions followed by long saturation phase. The saturation phase started at 4.07 MPa and after 4.5 s from the release onset. The minimum fluid temperature recorded was −17.8 °C in the reservoir and −78 °C in the 219.1 mm pipeline loop.
3. The mass release rate during the saturation period was steady. Using the differential pressure measurements, the mass release rate was estimated to be 788 kg s^{-1}.
4. With the low wind conditions in this test, the pseudo-steady CO_2 concentrations in the near field were similar at the upwind and downwind locations; whereas, in the far field pseudo-steady concentrations were not reached within the time frame of the release.
5. This large scale experiment could be used for further discharge and dispersion model validation and for further risk analyses of CO_2 pipeline.

Acknowledgements

References

Ahmad, M., Bögemann-van Os, M., Buit, L., Hulsbosch-Dam, C., Spruijt, M., Davolio, F., 2013. Study of the thermohydraulics of CO_2 discharge from a high pressure reservoir. Int. J. Greenh. Gas Control 19, 63–73.
American Conference of Governmental (Industrial Hygienists) ACGIH, 1991. Documentation of the Threshold Limit Values and Biological Exposure Indices, sixth ed. American Conference of Governmental Industrial Hygienists, Inc., Cincinnati, OH.
Brown, S., Martynov, S., Mahgerefteh, H., Proust, C., 2014. A homogeneous relaxation flow model for the full bore rupture of dense phase CO_2 pipelines. Int. J. Greenh. Gas Control 17, 349–356.
Cosham, A., Jones, D., Armstrong, K., Allason, D., Barnett, J., 2012. The decompression behavior of carbon dioxide in the dense phase. Paper No: IPC2012-90461 Proceeding of the 9th International Pipeline Conference.
Coooper, R., 2012. The National Grid COOLTRANS research programme. In: 3rd International Forum on the Transportation of CO_2 by Pipeline, Gateshead, UK.
CRS Report for Congress, 2007. Carbon Dioxide Pipelines for Carbon Sequestration: Emerging Policy Issues.
Dixon, C.M., Gant, S.E., Obiorah, C., Bilio, M., 2012. Validation of dispersion models for high pressure carbon dioxide releases. IChemE Symposium Series No. 158, IChemE, 153–163.
Hansen, O., Gilding, D., Nazarian, B., Osdal, B., Ringrose, P., Kristoffersen, J., Hansen, H., 2013. Snøhvit: the History of injecting and storing 1 Mt CO_2 in the fluvial Tubåen Fm. Enegie Procedia 37, 3565–3573.
Hill, T.A., Fackrell, J.E., Dubal, M.R., Stiff, S.M., 2011. Understanding the consequences of CO_2 leakage downstream of the capture plant. Energy Procedia 4, 2230–2237.
Mazzoldi, A., Hill, T., Colls, J.J., 2008a. CFD and Gaussian atmospheric dispersion models: a comparison for leak from carbon dioxide transportation and storage facilities. Atmos. Environ. 42, 8046–8054.
Mazzoldi, A., Hill, T., Colls, J.J., 2008b. CO_2 transportation for carbon capture and storage: sublimation of carbon dioxide from a dry ice bank. Int. J. Greenh. Gas Control 2, 210–218.
Mazzoldi, A., Hill, T., Colls, J.J., 2011. Assessing the risk for CO_2 transportation within CCS projects, CFD modelling. Int. J. Greenh. Gas Control 5, 816–825.
McGillivray, A., Wilday, J., 2009. Comparisons of risks from carbon dioxide and natural gas pipelines, HSE Research report RR 749. In: HSE Books. Health and Safety Executive, Sudbury http://www.hse.gov.uk/research/rrpdf/rr749.pdf
Metz, B., Davidson, O., de Coninck, H., Loos, M., Meyer, L., 2005. Carbon Dioxide Capture and Storage. IPCC. Cambridge University Press, UK, pp 431.
Pipeline Safety Instrument for COMAH Involving Pipelines, Joint Research Centre, European Commission, Major Accident Hazards Bureau, 1999. Ispra (Va) Italy.
Pohanish, P.R., Greene, S.A., 1996. Hazardous materials handbook. In: Carbon Dioxide. Van Nostrand Reinhold, pp. 330–331.

Wareing, C., Fairweather, M.M., Falle, S.A.E.G., Woolley, R.M., 2012. Reynolds-averaged Navier–Stokes modelling of sonic CO2jets. In: Hanjalic, K., Nagano, Y., Borello, D., Jakirlic, S. (Eds.), Proceedings of the 7th International Symposium on Turbulence, Heat and Mass Transfer. Begell House Inc., New York, pp. 349–512.

Wareing, C., Woolley, R.M., Fairweather, M., Falle, S.A.E.G., 2013. A composite equation of state for the modelling of sonic carbon dixoide jets in carbon capture and storage scenarios. AIChE J. 59, 3928–3942.

Wareing, C., Fairweather, M., Falle Woolley, R.M., 2014a. Validation of a model of gas and dense phase CO_2 jet releases for capture and storage application. Int. J. Greenh. Gas Control 20, 254–271.

Wareing, C., Fairweather, M., Falle Woolley, R.M., 2014b. Modelling punctures of buried high-pressure dense phase CO_2 pipelines in CCS applications. Int. J. Greenh. Gas Control 29, 231–247.

Witlox, H.W.M., Harper, M., Oke, A., 2009. Modelling of discharge and atmospheric dispersion for carbon dioxide releases. J. Loss Prev. Process Ind. 22, 795–802.

Witlox, H.W.M., Stene, J., Harper, M., Nilsen, S.H., 2011. Modelling of discharge and atmospheric dispersion for carbon dioxide releases including sensitivity analysis for wide range of scenarios. Energy Procedia 4, 2253–2260.

Woolley, R.M., Fairweather, M., Wareing, C.J., Falle, S.A.E.G., Proust, C., Hebrard, J., Jamois, D., 2013. Experimental measurement and Reynolds-averaged Navier–Stokes modelling of the near-field structure of multi-phase CO_2 jet releases. Int. J. Greenh. Gas Control 18, 139–149.

Woolley, R.M., Fairweather, M., Wareing, C.J., Proust, C., Hebrard, J., Jamois, D., Narasimhamurthy, V.D., Storvik, I.E., Skjold, T., Falle, S.A.E.G., Brown, S., Mahgrefteh, H., Martynov, S., Gant, S.E., Tsangaris, D.M., Economou, I.G., Boulougouris, G.C., Diamantonis, N.I., 2014. An integrated, multi-scale modelling approach for the simulation of multiphase dispersion from accidental CO_2 pipeline releases in realistic terrain. Int. J. Greenh. Gas Control 27, 221–238.